In Silico Modeling and Scoring of PROTAC-Mediated Ternary Complex Poses

Junzhuo Liao,[1] Xueqing Nie,[1] Ilona Christy Unarta,[2] Spencer S. Ericksen[3]* and Weiping Tang[1,2,3]*

Affiliations:

1. School of Pharmacy, University of Wisconsin-Madison, Madison, WI 53705, United States

2. Department of Chemistry, University of Wisconsin-Madison, Madison, WI 53706

3. Drug Development Core, UW Carbone Cancer Center, School of Medicine and Public Health, University of Wisconsin-Madison, 53705, United States

ABSTRACT: Proteolysis targeting chimeras (PROTACs) are bifunctional molecules that induce ubiquitination and subsequent degradation of proteins via formation of ternary complexes between an E3 ubiquitin ligase and a target protein. Rational design of PROTACs requires accurate knowledge of the native configuration of the PROTAC induced ternary complex. This study demonstrates that native and non-native ternary complex poses can be distinguished based on pose occupancy time in MD, where native poses exhibit longer occupancy times than non-native ones at both room and higher temperatures. Candidate poses are generated by MD sampling and pre-ranked by the classic MM/GBSA method. A specific heating scheme is then applied to induce ternary pose departure, generating an occupancy score and temperature score reflecting pose occupancy time and fraction. The scoring approach enables identification of the native pose in all the test systems. Beyond providing a relative rank of hypothetical poses of a given ternary system, the method could also provide empirical guidance to whether a given ternary pose is likely a native one or not. The success of the method is in part attributed to the dynamic nature of the pose departure analysis which accounts for solute entropic effects, typically neglected in the faster static pose scoring methods, while solute entropic contributions play a greater role in protein-protein interactions than in protein-ligand systems.

INTRODUCTION

Since the discovery of cell-permeable small molecule ligands of E3 ubiquitin ligases, such as Von Hippel-Lindau (VHL) and cereblon (CRBN), for targeted protein degradation,[1, 2] proteolysis targeting chimeras (PROTACs) have become valuable tools for dissecting cell biology[3] and also promising therapeutics[4-7]. PROTACs are bifunctional molecules having two ligands (warheads) connected covalently by a linker. One ligand binds to an E3 ubiquitin ligase, while the other ligand binds to the protein target. The formation of a target protein-PROTAC-E3 ligase ternary complex promotes ubiquitination of the protein target. Polyubiquitination in turn marks the target protein for degradation in the proteasome. Unlike traditional small-molecule ligands that usually modulate target protein function in bound state, PROTACs cause target degradation in a catalytic manner by a transient association with the target and thus produce a more sustained effect by target protein removal and require lower dosing.

PROTAC efficacy requires formation of target protein-PROTAC-E3 ligase ternary complexes. After a suitable ligand is developed for the target protein, it needs to be linked to an E3 ligase ligand appropriately to promote a competent ternary binding arrangement for subsequent ubiquitination of the target protein. It is therefore important to characterize and understand how the ternary complexes are formed. Accurate structure models of native ternary complex configurations are essential to structure-based PROTAC design and comparison of different PROTACs. However, obtaining a co-crystal structure from experiments is generally very time-consuming.

Computational approaches to PROTAC systems. Computational structure prediction methods have shown some potential for determining or characterizing native ternary complexes. A pioneering study in 2019 started with protein-protein docking as the first step, using the respective holo forms of the protein and ligand from the ternary crystal structure.[8] It is assumed that the two protein-ligand binary structures are available, and they remain unchanged in the native ternary complex. Independently generated

PROTAC conformers are then aligned to the ligand warheads in the protein docking poses. Energy minimization was then performed on the aligned PROTAC and used as an important filter. If the change of PROTAC poses due to minimization was sufficiently small, an indication of less PROTAC distortion generated during alignment, the ternary pose is predicted as crystal-like. A 40% hit rate was achieved in obtaining crystal-like poses for the $BRD4^{BD2}$-PROTAC-VHL ternary system (PDB: 5T35) (**Figure 1a** left, blue bar). However, it was also concluded that without prior knowledge of the crystal structures, it would be difficult to know *which* 40% are the correct poses given that the candidate poses are not scored. A 2020 update on this study used better filters and clustering to greatly improve the results for finding the native ternary pose of 5T35.[9] The largest cluster of predicted ternary poses almost completely corresponded to the native pose (**Figure 1a** left, green bar). However, the overall success rate for different systems is low (**Figure 1a**) and no other scoring was employed.

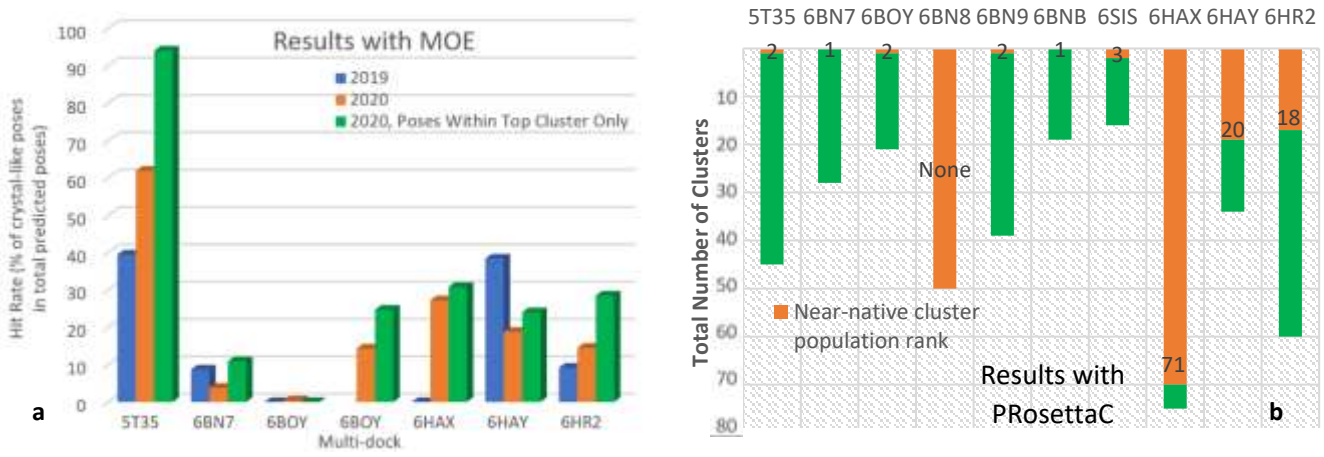

Figure 1. **a**. Previous search efforts using MOE from 2 studies combined, by Drummond *et al.* **b**. Reported results with the PRosettaC method by Zaidman *et al.* The population rank of the near-native cluster for each system is labeled. More green indicates a ranking closer to top, which is the ideal situation. More red indicates a ranking more deviated from top.

Another effort to determine native ternary complex structures used Rosetta-based modeling and provided improvements in accuracy and scope (**Figure 1b**).[10] Their method, PRosettaC, involves two rounds of protein docking and two rounds of Rosetta-based scoring to generate and filter ternary complex poses. Finally, the top 200 scoring poses are clustered with the cluster population rank being the final scoring criteria.

Indeed, these docking-based methods adequately search the conformation (configurational) space given that the native pose was almost always included in the resulting pose set. However, the pose filtering or scoring methods applied have not consistently identified the native pose across systems. In an ideal situation, the native pose should be ranked at the top across many different systems. If this issue is resolved, then low hit rates (or low cluster population of the near-native pose) as seen above would not be a concern anymore.

In the present study, we present a method for distinguishing native versus non-native PROTAC ternary complex poses using an MD-based scoring approach based on pose thermal durability. The scoring is effective not only on poses generated from our own conformation search results, but also on poses independently generated from other sources.

In our MD studies on PROTAC ternary systems, we have observed the native crystal ternary pose remain stable (occupying the starting state) throughout our simulations (up to ~100 ns long single trials), while non-native poses may or may not be stable during this time. Building on this observation, we convert pose occupancy parameters into general scoring of ternary pose stability. Scoring by such parameters provides a novel, effective and simple *in silico* method for evaluating the relative stability of hypothetical ternary poses. It can be performed in a practical manner by medicinal chemists with limited experience in setting up and running MD simulations.

To make the scoring approach more practical, the required simulation length is shortened by gradually increasing the kinetic energy of all the atoms (heating) in the system, to more rapidly destabilize candidate poses in each replicate run. Here we apply the scoring method to successfully predict the native pose on 4 structurally characterized ternary systems that we generated candidate poses on and which the native pose was among the candidates. The scoring is also effective on poses generated by other methods (i.e., PRosettaC).

There are two effects of heating on a general process of ligand dissociation RL ⇌ R + L, where R is receptor, L is ligand, RL is the bound complex, and at equilibrium $K = \frac{[R][L]}{[RL]}$. 1) Macroscopically, it increases the unbound-bound equilibrium constant K to favor unbound states more, as can be seen from the Van 't Hoff equation (1) where K increases with temperature.

$$ln\ K = -\frac{\Delta H° - T\Delta S°}{RT} = -\frac{\Delta H°}{RT} + \frac{\Delta S°}{R} \quad (1)$$

However, true observation of thermodynamic equilibrium can only be achieved with an ensemble of molecules, while simulation usually studies one complex. A ligand unbound from its pocket will be unlikely to rebind in simulation, and when it does, to the best of our knowledge there are so far no reports on any protein-ligand system of any size for which it was possible to use the unbound/bound population or time to obtain equilibrium K.[11-15] Thus, this study is by no means relying on or attempting to observe equilibrium shift of the ternary poses. 2) It decreases the occupancy time duration of the bound complex. Although this can be explained macroscopically by the Arrhenius equation, increasing the kinetic energy of every atom directly affects every microstate (or complex). Therefore, this decrease in bound occupancy time by heating is easily observed in simulation that is studying microstates/single complexes.

Heating has been demonstrated to accelerate protein unfolding simulations.[16-19] While in our case we are not unfolding the protein but even avoiding it, the ternary pose departure is clearly observed and accelerated. The protein structure itself is stable within our short MD trials, while ternary pose occupancy time was quite different for native vs non-native poses. At room temperature all candidate ternary poses are generally stable within the short tens of ns. With the pose occupancy time decreased to less than short tens of ns, one can easily compare different poses, as successfully demonstrated in this study.

While there are other techniques[20-25] capable of accelerating sampling which potentially includes ternary complex pose departures, heating is the simplest for the user and indeed worked very well in this specific PROTAC study. Additionally, there are two more advantages of this method. 1) It is performed in explicit solvent, avoiding the introduction and choice of a new set of parameters needed for the commonly used GBSA measurements. 2) This method inherently includes entropic effects to the evaluation of binding since one is looking at a dynamic process being run multiple times, instead of only the static molecular-mechanics (MM) energy values.

RESULTS AND DISCUSSION

The overall workflow of this study is summarized in **Scheme 1**. Based on the scoring of poses by our method, the native one is ranked at the very top. Although MD relaxations are involved in stage 1, the scoring in stage 2 and 3 does not rely on a specific sampling method and can be used independently as long as there are poses generated.

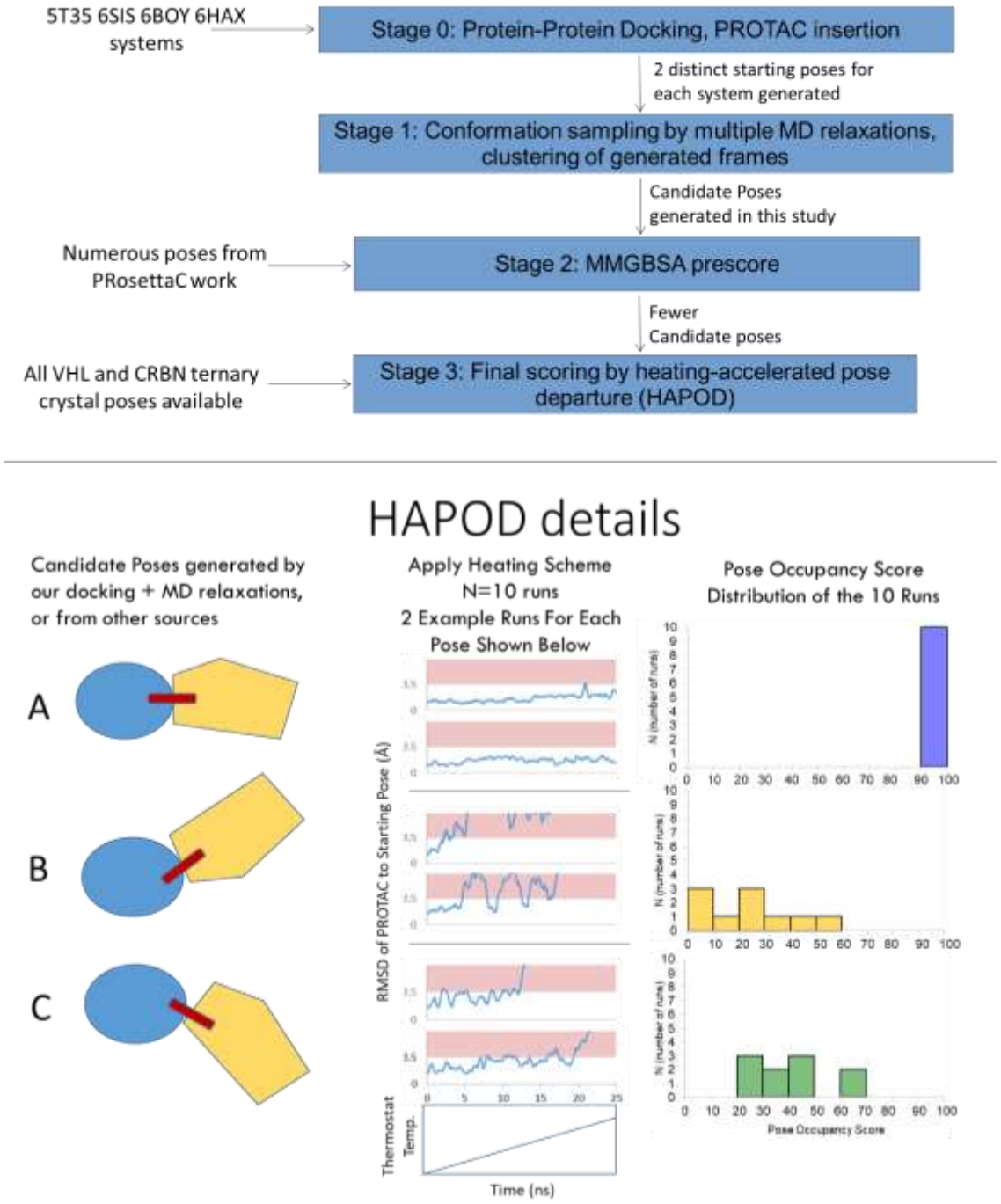

Scheme 1. Top: Overall workflow. Bottom: Summary of HAPOD scoring. In the bottom left, A is the best scoring and also native pose. Examples taken from 5T35 system (**Figure 4**). As in the bottom center plots, a 3.5 Å RMSD of the PROTAC ligand warhead to its start coordinates is the threshold we set for defining whether the ternary structure is still occupying the starting pose or not. The system temperature is

gradually increased in a linear way. The time duration of the RMSD measurement being within 3.5 Å is divided by the total time of 25 ns (then multiplied by 100), giving the occupancy fraction and score (bottom right).

Pretest Results

One advantage of MD search is that only poses belonging to a local energy minimum will remain stable, thus eliminating the majority of irrelevant, high energy poses. Though at the onset of this study, there were very few MD simulations on PROTAC systems.[26] Therefore, before the full workflow was established and numerous PROTAC systems were investigated, a pretest was first performed to examine the capability of MD along with the common choice of setups (most current forcefield, water, atomic partial charges), confirming if starting from a non-crystal pose that it can recapitulate the crystal pose, and that the crystal pose is stable in simulation. In the pretest, the search and scoring of BRD4-MZ1(PROTAC)-VHL (PDB: 5T35) using classic MD and MMGBSA was attempted (a simplified **Scheme 1** stage 0-2 only). The holo form proteins from 5T35 (see "Structure Preparation" and "Pretest" in the Experimental Section) were used to begin the modeling to keep the pretest simple. Encouragingly, two of each of the two sets of five runs converged onto the crystal pose. In the control run the crystal pose was stable over 110 ns.

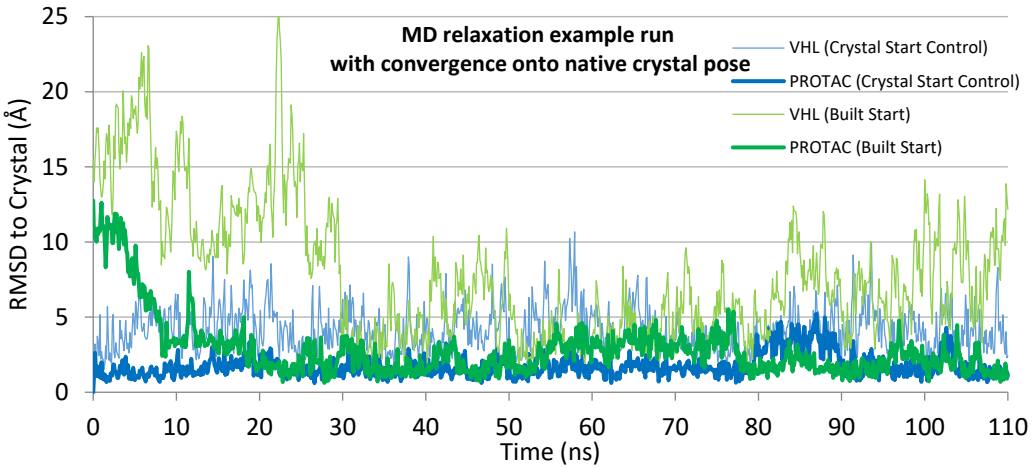

Figure 2. MD relaxation (1 example trial, 2-MD3 in **Table 1**) reaching convergence onto native crystal pose from built starting pose in the VHL-PROTAC-BRD4 (5T35) system. The BRD4 Cα were aligned to the crystal pose for every frame. PROTAC RMSD plotted based on VHL ligand warhead side. VHL RMSD was plotted based on its Cα.

The last 10 ns of the 10 total replicates + 1 control run was measured for MMGBSA ternary binding ΔH and cooperativity binding ΔΔH. Among the 4 runs that converged onto the crystal pose, along with a single control run starting from the crystal structure, these replicates had 5 out of 5 of the most favorable cooperativity binding enthalpies (ΔΔH) and 5 out of the 6 foremost favorable ternary binding enthalpies (ΔH) (**Table 1**). This encouraging result suggested that a quick local MD refinement is potentially capable of finding stabilized ternary poses, and a classic MMGBSA binding score may be useful to rank the native pose favorably.

Table 1. For the pretest using 5T35, four out of ten total MD relaxations converged on the native-like pose. The corresponding MMGBSA enthalpy energy calculations based on 10 ns time intervals at end of trajectories provide an effective ranking for distinguishing native versus non-native ternary poses. Error margin shown in s.e.m. All units in kcal/mol. 2-MD3 is the example trial shown in **Figure 2**.

Built Start Pose and Trial No.	Native pose convergence	Ternary binding enthalpy ($\Delta H_{bind,\ tern}$)	ΔH rank	Coop. enthalpy of ternary complex (ΔΔH)	ΔΔH rank

crystal starting pose	control	-117.5 ± 0.6	5.5	-25.3 ± 0.8	4.5
1-MD1	**YES**	-119.1 ± 1.1	5	-26.4 ± 1.5	4
1-MD4	**YES**	-119.3 ± 0.9	4	-32.1 ± 1.2	2
2-MD3	**YES**	-122.1 ± 0.9	3	-30.2 ± 1.5	3
2-MD4	**YES**	-122.3 ± 0.8	2	-32.7 ± 1.1	1
1-MD2	No	-112.6 ± 0.8	8	-14.5 ± 1.1	9
1-MD3	No	-105.3 ± 0.7	10	-11.7 ± 0.7	10
1-MD5	No	-127.4 ± 0.8	1	-21.1 ± 1.1	7
2-MD1	No	-113.9 ± 0.8	7	-21.7 ± 0.9	6
2-MD2	No	-105.8 ± 1.0	9	-15.7 ± 1.2	8
2-MD5	No	-115.7 ± 0.9	6	-22.4 ± 1.1	5

From this preliminary success, we expanded our scope of prediction to more ternary systems, including ones that failed from previously reported methods. Additionally, we also started docking from independent ligand-bound protein structures to better mimic the situation where no ternary crystal was available, not demonstrated in any of the 3 previous works on PROTAC ternary pose prediction.[8-10] Only during the preparation of this manuscript that the first method starting from independent binary and also apo protein structures was reported for the modeling of PROTAC-mediated ternary complexes.[27]

Sampling, Clustering and MMGBSA Prescoring Results

Expanding to four systems, in this stage, the sampled frames from the MD trajectories were analyzed by MMGBSA and clustered (**Scheme 1** Stage 1 and 2, also see "Conformation Sampling" and "MMGBSA Prescore" parts in the Experimental Section). Clustering frames based on protein and PROTAC coordinates helps us to determine 1) pose convergence in a given replicate, and 2) pose convergence from independent replicates. **Figure 3** shows clustering analysis for 5T35. Clustering for 6SIS, 6BOY, 6HAX are shown in SI, **Figures S7-S9**. In the graphs, the trials are denoted as numbers x.y, where x indicates the starting pose number and y indicates the MD trial number for that start pose.

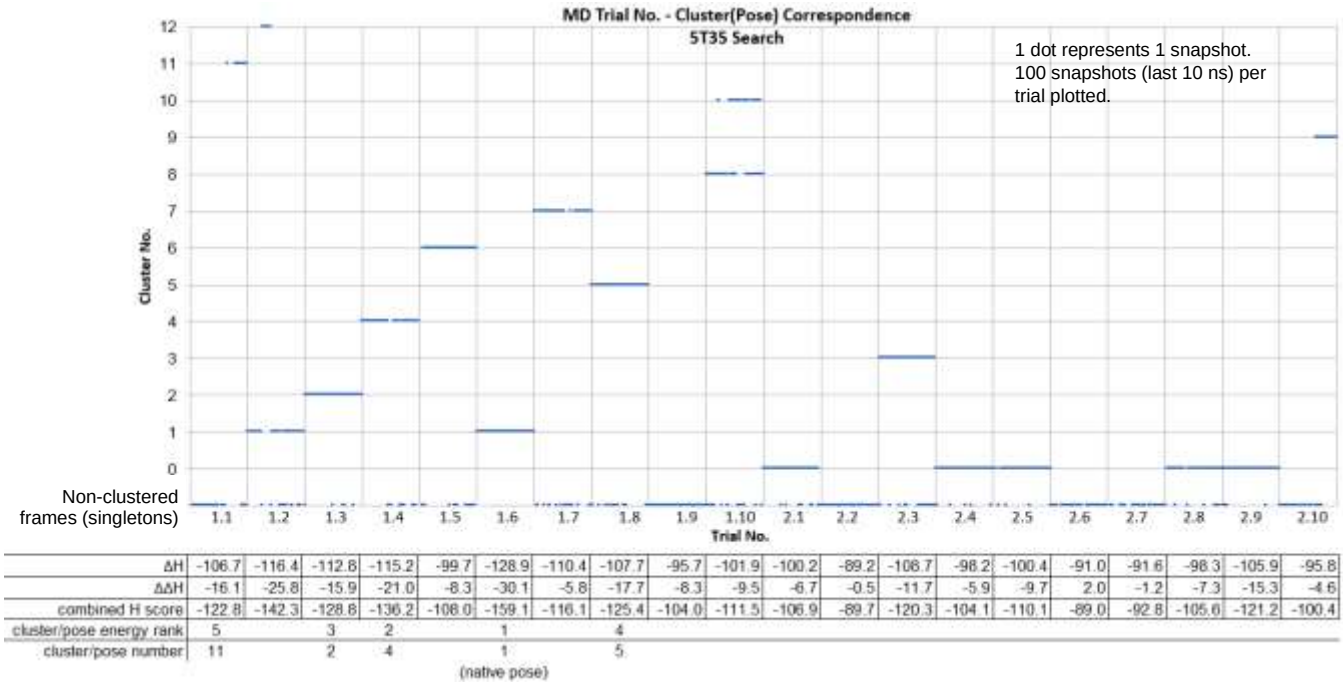

Figure 3. Clustering analysis of the last 10 ns from all 20 simulations for the 5T35 system (2 starting poses, 10 replicates each). 1.x are trials starting from pose 1 and 2.x are trials starting from pose 2. The corresponding MMGBSA energy for each run is shown below. For every cluster, if all member frames were derived from the same replicate (e.g., cluster no.2), its representative pose is assigned the H score of this replicate's trajectory (-128.8). If more than one trajectory converged on a given cluster (e.g., cluster no.0), the representative pose is assigned the most favorable H score among the replicates that converged on the cluster (-121.2 from trial 2.9).

The searches for 5T35 and 6SIS involving VHL from an independent crystal found the native ternary quickly within the initial set of 10 replicates per pose. Based on the criteria of requiring the trajectories to converge onto the lowest enthalpy pose from more than 1 replicate, 6SIS was given an additional 10 runs for the second starting pose (**Figure S7**).

6BOY being larger than the rest was observed to move slower than desired when first ran in explicit solvent. To speed up sampling, implicit solvent was used which has a much faster conformation search

speed due to lack of solvent viscosity.[28, 29] With the increased solute flexibility, we restricted specific internal degrees of freedom: 1) CRBN was held rigid at all atoms 2) PROTAC warheads were held in the binding pocket 3) BRD4 was internally restrained at Cα. Without such restraints, the proteins were too flexible to converge on the native crystal pose within the trajectory lengths. By imposing such restraints, only the holo form proteins from 6BOY ternary converged on a native pose. The available independent conformer of CRBN-ligand in binary complex (i.e., PDB: 4TZ4) departs significantly from the ternary complex (6BOY) at one region of the binding interface.

While 6HAX with independent binaries starting from docking also did not reach the crystal pose within the search trials we attempted, the holo form proteins from the ternary with MD start pose artificially modified from the ternary crystal (to a distance of VHL Cα RMSD of 11.79 Å, and VHL warhead RMSD of 7.11 Å) did consistently find the native pose, among other poses, generating a good set of candidates for subsequent scoring testing. Poses found from both starting versions (last row, **Table 5, Experimental Section**) were later jointly compared of their MMGBSA scores. Since two poses from the independent binary starting version had an even lower enthalpy score than the found native (**Table 2d**), they were good candidates to test our final rescoring (**Figure 4** 6HAX, poses ind. bi.+dock.0 and 1).

Table 2. MMGBSA prescoring results. Enthalpy measures were taken over the last 10 ns of the trajectory corresponding to each candidate pose. If multiple trajectories converged on a pose based on clustering the most favorable trajectory result is reported for the candidate pose. All units in kcal/mol. Uncertainty reported as standard error of mean (s.e.m.).

a. 5T35

candidate pose # to be rescored with HAPOD	ΔH	ΔΔH	combined score (ΔH+ΔΔH)
1 (found native pose)	-128.9±0.8	-30.1±0.6	-159.1±1.3
4	-115.2±0.8	-21.0±0.5	-136.2±1.2
2	-112.8±0.7	-15.9±0.5	-128.8±1.1
5	-107.7±0.7	-17.7±0.5	-125.4±1.1
11	-106.7±1.1	-16.1±0.8	-122.8±1.8

b. 6SIS

candidate pose # to be rescored with HAPOD	ΔH	ΔΔH	combined score (ΔH+ΔΔH)
3 (found native pose)	-120.9±0.7	-30.4±0.5	-151.3±1.1
1	-112.3±0.8	-15.6±0.7	-127.9±1.4
4	-116.8±0.9	-6.9±0.5	-123.8±1.3
11	-112.1±0.7	-8.2±0.6	-120.3±1.1
9	-107.0±0.7	-12.9±0.5	-119.9±1.1

c. 6BOY

candidate pose # to be rescored with HAPOD	ΔH	ΔΔH	combined score (ΔH+ΔΔH)
0	-89.2±0.5	-22.9±0.5	-112.1±1.0
3 (found native pose)	-84.6±0.5	-16.1±0.3	-100.7±0.7
5	-83.4±0.6	-15.8±0.5	-99.1±1.0
4	-84.9±0.5	-12.5±0.3	-97.4±0.7
2	-83.1±0.5	-10.1±0.4	-93.1±0.8
1	-73.8±0.4	-8.9±0.3	-82.7±0.6

d. 6HAX

candidate pose # to be rescored with HAPOD	ΔH	ΔΔH	combined score (ΔH+ΔΔH)
ind. bi. + dock.0	-106.3±0.9	-12.5±0.7	-118.8±1.6
ind. bi. + dock.1	-102.0±0.7	-12.5±0.5	-114.5±1.1
0 (found native pose)	-102.2±0.9	-10.1±0.7	-112.3±1.5
4	-92.5±0.6	-12.5±0.5	-105.0±1.1
1	-94.4±0.5	-7.5±0.3	-101.9±0.6
2	-97.9±0.5	-3.8±0.2	-101.7±0.2
11	-91.3±1.0	-9.6±0.8	-100.9±1.7

While MMGBSA enthalpies for 5T35 candidates poses rank the found native pose corresponding trajectory at the top, it failed for 6BOY (**Table 2a** and **c**). An RMSD-energy funnel plot (**Figure S10**) further corroborated that there were other configurations with lower computed binding enthalpy than the found native pose. This could be due to inaccuracy in the MMGBSA estimation. At the same time, it is also known that protein-protein binding free energies have large entropy contributions.[30] When entropy calculations were included on the 6BOY system (SI **Table S2,** on a different set of earlier results but with same poses found), it did improve the rankings. The entropy calculation was by normal mode analysis with a subset of frames. While adding the entropy improved the binding score of the found native poses somewhat, at the same time the size of the system made the calculations only marginally practical to perform, even after partially adapting the method reported by Ryde et. al.[31] to prune the protein.

Since entropy is essentially related to the probability of an energy configuration being reached, direct accurate calculation of entropy can only be obtained macroscopically via eq. (1). When focusing on a single complex, there are numerous ways to work around this, such as normal mode vibrational analysis (as performed above) and thermodynamic integration (TI)[32, 33] for direct calculation of free energy change (ΔG) avoiding separate calculation of entropy. Nonetheless, they are still limited in various ways. TI needs to be a slow process for small changes between two states, which is not suitable for large conformation changes. Calculation of normal mode vibrational frequency is extremely computationally demanding with

a large margin of error, and it is more accurate for gas phase than solution phase.[34] So it is not surprising that entropy calculations are often neglected for *in silico* drug discovery.

While only using MMGBSA enthalpies are insufficient to score poses in some systems, and quantitative entropy calculations are too computationally demanding and also inaccurate, the enthalpy score remains useful for prescoring of candidates poses since the native poses were generally still favored. **Tables 2a-d** show the top scoring poses. The full MMGBSA enthalpy results are listed at the bottom of the clustering results, **Figure 3** bottom, and **Figure S7-S9** bottom.

Final Rescoring by Heating-Accelerated Pose Departure Trials (HAPOD)

After the number of candidate poses are reduced, the final ranking of the poses are determined by our HAPOD method (**Scheme 1** bottom, see also Introduction and "Final Rescore by Heating-Accelerated Pose Departure Trials (HAPOD)" in the Experimental Section). As established and presented, our simple and optimized way of running the heating trials is by gradually heating the system from 310 K to 410 K over a short 25 ns, with ten replicates sufficient to distinguish the rank of poses in most system. HAPOD successfully corrected the MMGBSA rankings of the found natives and ranked each at the top for all four systems (**Figure 4**). Both the occupancy score and temperature score (T) (see "Generating scores from HAPOD" part in Experimental Section) provided similar pose rankings, with the occupancy score being marginally better. The T score was included so that one can estimate at what temperatures the pose departures are occurring.

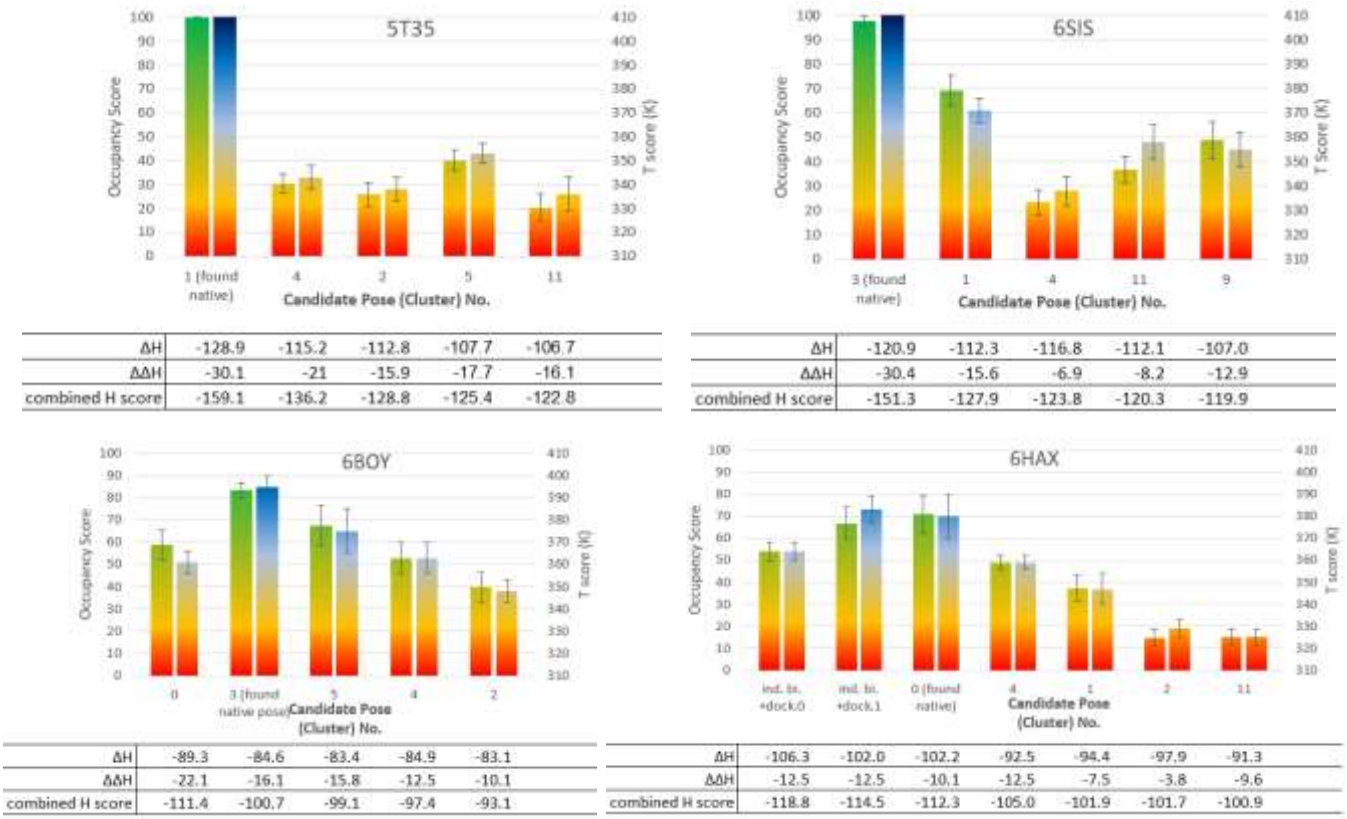

ΔH	-128.9	-115.2	-112.8	-107.7	-106.7
ΔΔH	-30.1	-21	-15.9	-17.7	-16.1
combined H score	-159.1	-136.2	-128.8	-125.4	-122.8

ΔH	-120.9	-112.3	-116.8	-112.1	-107.0
ΔΔH	-30.4	-15.6	-6.9	-8.2	-12.9
combined H score	-151.3	-127.9	-123.8	-120.3	-119.9

ΔH	-89.3	-84.6	-83.4	-84.9	-83.1
ΔΔH	-22.1	-16.1	-15.8	-12.5	-10.1
combined H score	-111.4	-100.7	-99.1	-97.4	-93.1

ΔH	-106.3	-102.0	-102.2	-92.5	-94.4	-97.9	-91.3
ΔΔH	-12.5	-12.5	-10.1	-12.5	-7.5	-3.8	-9.6
combined H score	-118.8	-114.5	-112.3	-105.0	-101.9	-101.7	-100.9

Figure 4. HAPOD scoring on poses from 4 ternary systems. These reduced number of candidate poses are determined from MMGBSA prescoring. Left bar shows occupancy score, right bar shows temperature score (T). Error bars show s.e.m. Corresponding MMGBSA energy scores for each pose shown at bottom of each graph, the same values as in **Tables 2a-d**.

Notably, part of the success of HAPOD may be attributed to the fact that the protein structure themselves were all stable during our short trials. The short run times and not too high heating ceiling (410 K) may have also helped, keeping the water molecules all liquid. To better understand these features, we examined solvent and solute stability under the simulation conditions. To assess the behavior of OPC water at elevated temperature, we monitored the system density throughout the heating scheme (**Figure S11**). The bulk system density shows no abrupt changes signaling instability or phase transitions over the heating scheme, indicating the water still well solvating the solute.

Protein structural stability as a more important concern was also monitored over the course of the heating. Protein unfolding or other significant protein structural deformation during the HAPOD scoring may mask the change of the ternary pose, making all poses score like poor ones. Therefore as control measures the protein stability was always monitored in the HAPOD scoring. Fortunately, the RMSD of the aligned protein rarely increased to more than 3 Å (SI **Figure S12**) from the starting pose. If the protein does unfold, adding internal restraints to the protein will be a simple solution although it is not involved in this study.

We then examined the potential of HAPOD scoring to address an important but unresolved issue with PROTAC-ternary pose prediction methods. In the absence of a known ternary crystal structure, how do we know a native ternary pose exists among candidates poses? While scoring methods always enable a relative ranking of poses, available scoring methods, to our knowledge, do not indicate whether in a set of candidate poses, the native one exists or not. Results of HAPOD scoring within the same ternary system and across different systems indicated that the four crystal ternary poses all show an occupancy score of >70 and T score >380 K, while non-native poses generally did not. Looking further into this finding, we applied HAPOD to measure occupancy and T scores for all the available VHL and CRBN-containing ternary crystal structures.[35]

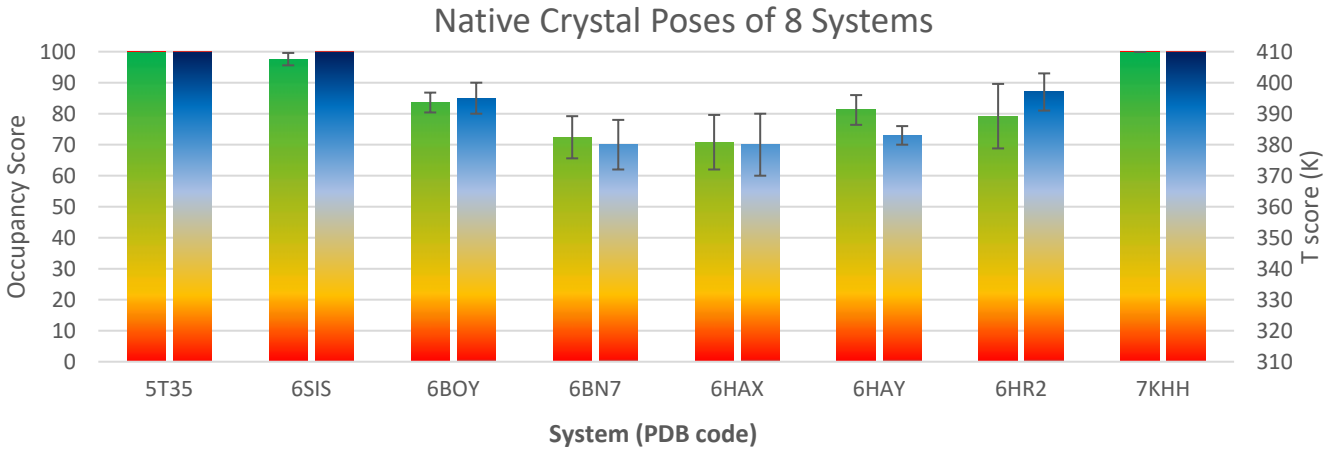

Figure 5. Scores of all resolved crystal structures. 5T35, 6SIS, 6BOY, and 6HAX scores from found native pose in our study. 6BN7, 6HAY, 6HR2 and 7KHH scores measured from crystal PDB pose. Error bars show s.e.m.

All of these native ternary systems show occupancy and T scores above 70 and 380 K, respectively (**Figure 5**). From these results we empirically propose these HAPOD score thresholds as a criteria for native-likeness of candidate poses, given the same simulation conditions as in this study. Run conditions are described in the Experimental Section and input scripts along with all structures are available on GitHub[36].

HAPOD Scoring on Independently Generated Candidate Ternary Poses

The MD-based conformation search procedure used in this study only covers a limited configurational space. The process of reaching the native within a short amount of time is quite dependent on docking to get a good starting point, though partial success was obtained even with independent binary crystals as the inputs. The final HAPOD scoring is exceptionally successful in distinguishing native from non-native ternary poses and can be used independently from our MD-based pose sampling, just like using the crystal coordinates as inputs demonstrated above. To examine the utility of HAPOD scoring on poses generated by other search methods, PRosettaC-generated poses were evaluated.[10, 37]

For the two systems of 6BOY and 6HAY being evaluated, all poses originally ranking higher than their near-native were scored (**Figure 1b**). For 6BOY this meant only 3 poses (including a crystal native control) are subject to HAPOD rescore, however for 6HAY there were much more, being 21. Routinely scoring over 20 poses by HAPOD is still time consuming and unnecessary, therefore an MMGBSA prescore is applied to eliminate some poses first. Unlike in the conformation search stage, we are scoring given poses and not searching for new poses. In addition, there is not an MD trajectory already available to extract

MMGBSA energies from. So for the above two reasons, in the PRosettaC rescore, single-frame MMGBSA energy calculations from minimized structures are applied (which has also been commonly used in literature with success[38-40]). This also allows the MMGBSA computation time to be less than 3 minutes per pose on a local mid-level GPU. Results and some structural analysis of 6HAY (SMARCA2(BD)-PROTAC-VHL) poses are shown in **Table 3**.

Table 3. MMGBSA energy prescoring of all 6HAY poses that originally ranked ahead of the near-native, the near-native pose itself and the crystal pose. Poses taken for HAPOD rescore are marked with a check. Structural issues were detected for several poses marked out with asterisks.

Original Cluster Number and rank	ΔH	ΔΔH	combined H score	Taken for HAPOD rescore
10	-141.3	-58.2	-199.6	**
8	-128.5	-47.4	-175.9	✓
16	-131.4	-43.4	-174.8	✓
2	-130.6	-41.3	-171.9	✓
11	-130.1	-38.5	-168.6	✓
6	-119.1	-35.4	-154.5	✓
crystal	-126.5	-25.6	-152.1	✓
5	-121.9	-29.3	-151.2	✓***
14	-112.1	-37.8	-150.0	*
4	-125.4	-20.2	-145.6	✓
20 (near-native)	-120.7	-23.5	-144.1	✓
15	-116.8	-25.0	-141.8	
17	-111.6	-30.1	-141.7	
12	-112.3	-27.6	-139.9	
13	-117.5	-21.9	-139.3	

1	-109.5	-27.4	-136.9	✓
7	-108.6	-22.2	-130.8	
18	-107.7	-13.5	-121.1	
3	-105.5	-14.1	-119.6	✓
19	-101.4	-13.7	-115.1	
9	-102.4	-11.5	-113.9	

*Artifactual pose. The SMARCA2(BD) protein domain is situated almost parallel to VHL, causing the known VHL anchor proteins (EloB and C) forming the VBC complex to directly clash with BD (see SI **Figure S13**). However, the PRosettaC modeling did not consider this information and generated a pose anyway.

Pose similar to 14, also artifactual. Even though the atoms in the model do not directly clash with VBC like in pose 14, they were still close in vicinity and the residues immediately extending out of the C-terminal of resolved SMARCA2(BD) is likely to clash with VBC. These are residues not in the crystal-resolved BD domain. The full SMARCA2 protein structure is obtained by AlphaFold prediction (AF-P51531-F1).[41] The full SMARCA2 protein will also clash with VHL. See SI **Figure S14 (top) for pose. By comparison, the full SMARCA2 protein aligned to the 6HAY crystal structure does not at all clash with VBC. To further test the credibility of the AlphaFold predicted structure of full SMARCA2, the constructed SMARCA2-VBC complex was expanded in the other direction. The E3 complex (from PDB: 5N4W) was aligned to VBC in 6HAY. This generated the full target protein-full E3 complex structure, and it is able to be formed comfortably without any clash or hindrance, verifying an overall credibility of the AlphaFold full SMARCA2 prediction. See **SI Figure S14** (bottom) for pose.

***Full SMARCA2 could clash with VHL based on the same AlphaFold prediction used above for pose 14, but since evidence was not as strong, this pose is not eliminated from HAPOD rescore.

The original top 5 PRosettaC ranked poses, and all poses with an MMGBSA combined H score better than the near-native, except for the ones being unrealistic artifactual poses (10 and 14) were taken for HAPOD rescore. From the structural analysis of PRosettaC 6HAY poses, it is worth mentioning that in reality proteins do not exist as standalone domains, but most modeling usually studies a certain domain. Artifactual modeling results should be eliminated whenever it is detected.

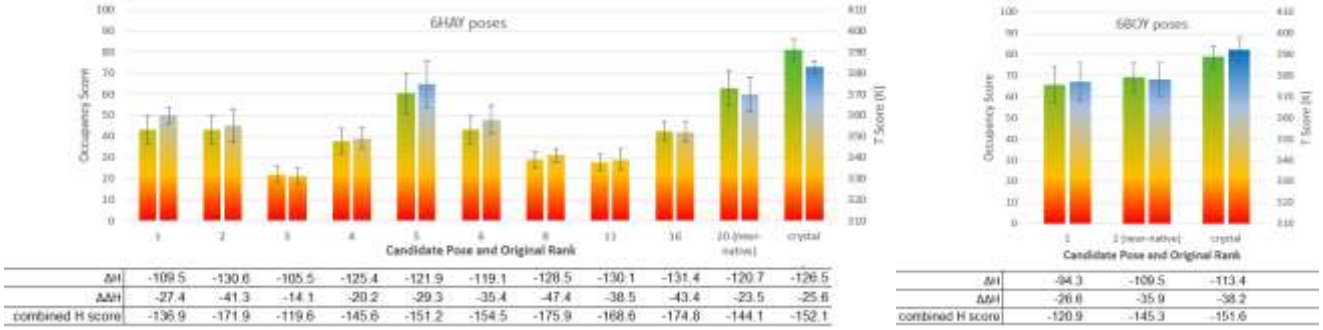

	1	2	3	4	5	6	8	13	16	20 (near-native)	crystal
ΔH	-109.5	-130.6	-105.5	-125.4	-121.9	-119.1	-128.5	-130.1	-131.4	-120.7	-126.5
ΔΔH	-27.4	-41.3	-14.1	-20.2	-29.3	-35.4	-47.4	-38.5	-43.4	-23.5	-25.6
combined H score	-136.9	-171.9	-119.6	-145.6	-151.2	-154.5	-175.9	-168.6	-174.8	-144.1	-152.1

	1	2 (near-native)	crystal
ΔH	-94.3	-109.5	-113.4
ΔΔH	-26.6	-35.9	-38.2
combined H score	-120.9	-145.3	-151.6

Figure 6. HAPOD rescore of top candidate poses from PRosettaC. Pose no. indicate original rank based on cluster population. Error bars show s.e.m. over 10 replicates.

Originally, the near-native pose for 6BOY was ranked 2nd (out of 22), and 6HAY was ranked 20th (out of 35) based on PRosettaC method. By calculation of MMGBSA binding enthalpies for the poses obtained from PRosettaC, we observed that the ranking of the near-native poses improved somewhat (**Table 3** and **Figure 6** bottom). But based on MMGBSA energy some poses from PRosettaC were also enthalpically more favored than the native. In such case, it will be less surprising that they will rank ahead of the near-native pose based on static energy techniques. The HAPOD method mostly corrected the pose ranks (**Figure 6**). All of the non-native poses that originally ranked in the front scored less favorably than the near-native pose based on the occupancy score, excluding two statistical ties not distinguished within 10 runs (one of them, 6HAY pose 5 was a suspected artifactual pose, see **Table 3**). The native crystal pose clearly scored the best. There was a small scoring difference between the near-native and the crystal native. Deviations between the near-native poses and crystal poses were small with respect to Cα RMSD, but fewer protein-protein and protein-PROTAC contacts were observed in the near-native pose (**Table 4**).

Small differences in sidechain contacts were sufficient to produce small but significant differences in HAPOD scoring. A pose is not ideal enough if the side chains are not within proper intermolecular contacts. The crystal structure is one example of having good contacts.

Table 4. A comparison of the number of intermolecular atom contact pairs in crystal structures and found natives. Contacts were defined by a Van der Waals surface distance of < 0.4 Å.

Complex	Molecule Pair:	CRBN-BRD4	BRD4-PROTAC	PROTAC-CRBN
6BOY Crystal		84	61	83
6BOY near-native (pose 2, **Figure 6** right)		65	29	69
6BOY found native from own study with MD search		63	44	61
Complex	Molecule Pair:	VHL-BD	VHL-PROTAC	PROTAC-BD
6HAY Crystal		45	85	125
6HAY near-native (pose 20, **Figure 6** left)		43	84	103

CONCLUSION

The prediction of an accurate ternary pose is essential for structure-based PROTAC design when the structure of the ternary complex is not available. This study examines feasible strategies for predicting PROTAC-mediated ternary poses *in silico* in the absence of a known ternary co-crystal structure. We have developed a novel way to score such hypothetical ternary complex poses by heating-accelerated pose departure (HAPOD) trials of candidate poses with explicit solvent MD, and measuring its average pose occupancy fraction while subject to gradual heating. It is highly successful in the systems available for testing. Candidate poses in this study were first generated by protein docking and short MD conformational searches. Later on, more poses from other sources were also included as candidates. The HAPOD scoring method here fills in an important gap of which previous PROTAC ternary complex prediction models did not address or addressed poorly by relying on enthalpy-based static scoring techniques.

Our method accounts for both enthalpic and entropic contributions to ternary complex stability. Entropy is especially important when protein-protein interactions are involved. It therefore provides a much more complete picture based on the success in all the systems we examined here. The process is relatively straightforward, self-intuitive, and easy to use for medicinal chemists without extensive experience in MD. Even with repeated heating replicates, the calculations are much faster than performing normal mode entropy calculations for systems of this size with a huge interface. While MMGBSA enthalpy is still used for prescoring, the final HAPOD rescore is run in explicit solvent without involving a choice of another set of GB parameters. We anticipate that our HAPOD scoring method combined with MD search or other means of conformation sampling for native ternary pose determination will provide useful assistance to the structure-based rational design of PROTACs.

EXPERIMENTAL SECTION

Structure Preparation and Pretest

Protein docking. Protein-protein docking poses were first obtained using ClusPro,[42-44] which is simple to use as a free online server. For the design of most PROTACs, the two ligand warheads and their binding pockets are already known from crystal structures of their binary complexes. For docking input, we used the holo form protein structures from independent protein-ligand binary crystals or the ternary crystal. The ligands were not included in the docking input since they are not recognized by ClusPro. Residues around each ligand pocket were specified as attractive regions in the ClusPro Options to favor close proximity of the ligand binding sites in the two proteins (**Table 5**). Output results may still include poses that have the two pockets too far for linker attachment, even with the specified attractions. These poses were excluded for further use. Of the remaining, the top two ClusPro "balanced" scoring poses were selected.

Table 5. Attraction residues specified for each system in ClusPro. Residues were selected based on proximity to where the PROTAC linker would be connected. The smaller protein was defined as "receptor" to afford greater flexibility in the larger protein. Cluspro allows some backbone and sides chain flexibility in the ligand, but the backbone is held rigid in the receptor. The single letter followed by number is the chain ID and residue number in the input PDB.

System	Receptor	Ligand	Input PDB when independent binary crystal was used instead of holo protein from ternary
5T35[26]	$BRD4^{BD2}$ a-433, 385, 432	VHL c-67, 91, 69	4W9H (VHL-ligand), independent $BRD4^{BD2}$-ligand unavailable
6SIS[45]	$BRD4^{BD2}$ a-433, 385, 432	VHL c-112, 109, 98, 90	4W9H (VHL-ligand), independent $BRD4^{BD2}$-ligand unavailable
6BOY[46]	$BRD4^{BD1}$ c-87, 146, 140, 83	CRBN b-357, 386, 352	-
6HAX[47]	$SMARCA2^{BD}$ a-1413, 1463, 1470	VHL c-98, 99, 108, 110	5NVX (VHL-ligand) and 6HAZ ($SMARCA2^{BD}$-ligand)

PROTAC insertion. The linkers were cut as indicated (**Figure 7**). To regenerate the linker in 3D, either conversion from its SMILES string by *omega2*[48, 49] or building it visually in Chimera[50] was performed.

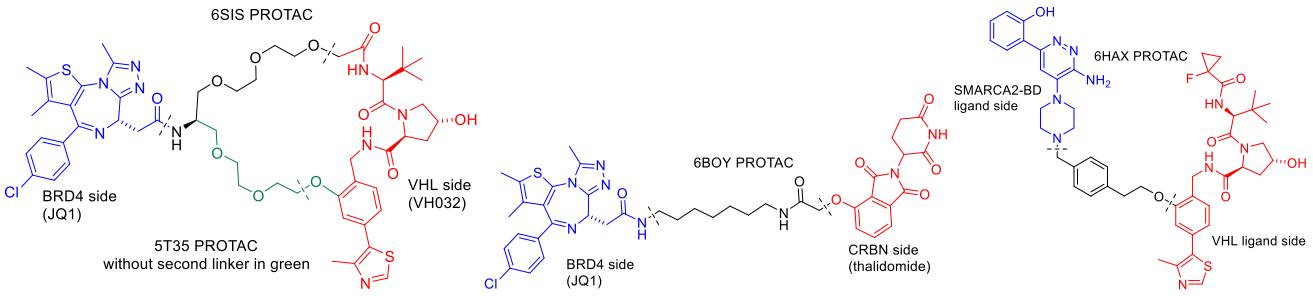

Figure 7. PROTAC chemical structures and cutting points during 3D model building.

Using Chimera,[50] in each protein-protein docked pose, ligand warhead placements into their respective pockets were based on the crystal structures. Since the PROTAC was not in the docking stage, some minor translational adjustment of the protein (mainly perpendicular to the protein contact plane) was applied

based on visual inspection to provide sufficient space for the PROTAC linker to avoid clashes with the 2 proteins structures. The linker was then attached manually. To remove distorted bond lengths and angles of the attached linker, we proceeded first without considering the proteins. To this end, 100 steps steepest descent + 10 steps conjugate gradient minimization was performed 10 times on the linker. When the proteins are included, another 100 steps steepest descent + 10 steps conjugate gradient minimization steps were performed 10 times. Only linker atoms and on one occasion a single protein side chain that is too close to the linker were allowed to move. In this step one does not need to worry about minor randomness of the starting pose due to model building, because the subsequent MD relaxations should not and is not sensitive to these small starting condition changes. SI **Figure S6** includes 3 distinctively different starting poses of VHL from different instances of model building, all which converged onto the native pose. More detailed step-by-step model building procedures which were performed in Chimera are provided in the SI.

Preparation for MD. AM1-BCC charges were assigned to the PROTACs by *antechamber*.[51] The *gaff2* forcefield was used for the PROTAC and parameters assigned by *parmchk2*. In *tleap*, the ff19SB force field was used for proteins.[52] An octahedral box of OPC water extending at least 10 Å from solute atoms was generated.[53] Na^+ and Cl^- counterions were added to neutralize the system.[54] Hydrogen-mass-repartitioning (HMR) assigning solute hydrogens a mass of 3.024 was used to enable a 0.004 ps timestep, or 0.002 ps at higher temperatures.[55]

In our pretest stage when the newer ff19SB was not yet released, *gaff* for PROTAC, ff14SB for proteins,[56] and TIP3P water was used.[57] There were no differences in the results with either setup. All final results reported here are with the newer ff19SB setup.

For implicit solvent simulations (6BOY) and MMGBSA energy calculations, mbondi2 radii set and GB^{OBC2} (igb=5) model was used.[58] HMR was not applied.

Pretest. VHL-PROTAC-BRD4 (PDB: 5T35) was examined as a pretest starting with a single GTX 1070Ti graphics card on a local workstation. After a short routine minimization and equilibration stage, 110 ns of MD relaxation at 310 K was applied to the two built starting poses (**Table 5** row 2, when using holo form proteins from known ternary), each given 5 replicates. Another control run was performed using the crystal ternary as the starting pose to examine pose stability and for subsequent energy scoring. Later when more systems were tested, 5T35 was included again, following the established procedures of this study separate from the pretest.

Conformation Sampling

The sampling started out with 10 relatively short runs (or 30 for implicit solvent 6BOY) per pose and was increased accordingly based on the scoring results (**Table 6**). This starting point was determined based on our pretest experience, hardware limits and literature reports on multiple short runs being better than a single long run[15, 59]. The GPU version of AMBER (*pmemd.cuda*) was used in all simulations reported in this study.[60-63]

Table 6. Actual sampling amount

System	No. of starting poses	Simulation time for each single replicate	Final replicates for each start pose
5T35	2	50 ns	x10
6BOY	2	20 ns (GB^{OBC2} (igb=5))	x30
6SIS	2	50 ns	x10 for pose 1, x20 for pose 2
6HAX	1+1	50 ns	x20

For each system, we required to have at least two trajectories converge onto the most favored MMGBSA prescore pose, as determined over the last 10 ns of the trajectories. If only one trajectory converged onto the lowest MMGBSA prescore pose, the number of replicates is then increased. This mimics the situation when there is no prior knowledge of the ternary crystal pose, and only scoring results are available from trajectories. Additionally, the final HAPOD rescore later in this study can be used to further guide the

amount of sampling both in terms of starting pose numbers and simulation trials, if no pose achieved HAPOD scoring of a >70 occupancy score and >380 K temperature score, empirically drawn from examining all the currently available CRBN and VHL ternary crystals.

Explicit solvent MD trials. A short minimization and equilibration stage was performed proceeding the production stage, with 5,000 steps of steepest descent minimization (ntmin=2) with heavy atoms restrained at 5 kcal/mol/Å, followed by MD equilibration in the NPT ensemble (ntb=2, ntp=1, Monte Carlo barostat, barostat=2, taup=0.5, thermostat=Langevin, ntt=3, gamma_ln=2) at 310 K for 150,000 steps (0.001 ps timestep), with heavy atoms restrained for the first 50,000 steps at 5 kcal/mol/Å. Complete force evaluation was applied (ntf=1, ntc=1). The minimization and equilibration conditions were initially adapted from the Rizzo group[64] and gradually modified throughout the course of this study. The production stage of 50 ns was run in the NVT ensemble (thermostat=Langevin, ntt=3, gamma_ln=0.01). The long-distance cutoff was set to 8 Å. The SHAKE algorithm was imposed to restrict hydrogen bond length changes, and no forces are calculated for bonds with hydrogens (ntc=2, ntf=2). The timestep was set to 0.004 ps, and snapshots were recorded every 0.1 ns.

Implicit solvent MD trials. This procedure applies to the 6BOY search. GB^{OBC2} was used (igb=5). After allowing hydrogens to fully minimize while heavy atoms were restrained by force constant of 5 kcal/mol/Å over 5,000 steps steepest descent (ntmin=2), CRBN and its ligand warhead were held mostly rigid by weight restraints of 10 kcal/mol/Å on all atoms. BRD4 was held by internal distance restraints of all Cα atoms to a single Cα based on the starting pose. The BRD4 ligand warhead was held in its pocket by distance restraints. Based on the starting pose atom distances, the distance restraints were a parabola well generated in *cpptraj* 1 Å wide and extending up linearly outside the parabolic well region. The force constant for restraint was 10 kcal/mol/Å. MD equilibration at 310 K for 250,000 steps (0.001 ps timestep) with complete force evaluation was applied (ntf=1, ntc=1) after the minimization stage. The production

stage was run for 20 ns. The SHAKE algorithm was applied. The Langevin thermostat (ntt=3, gamma_ln=2) was used. No long-distance cut-off was applied. The timestep was set to 0.002 ps, and snapshots were recorded every 0.1 ns.

Combined clustering of frames. For each system, all frames from the last 10 ns of each MD run were combined and clustered based on solute coordinates. Prior to clustering, in each trajectory the smaller BRD4 (or BD) was aligned to its crystal structure. Coordinates of the other protein's Cα (excluding the region bound to the deleted anchor proteins) and its ligand warhead heavy atoms were used to calculate the RMSD for clustering. Aligning the smaller protein helped make the movements and differences more prominent in the analysis. The DBSCAN algorithm was used and the Epsilon was set to 1.5 Å and minpoints set to 1. No sieving was used so all frames were used to cluster. *Cpptraj* was the program used to cluster and extract poses.[65]

For each cluster, one representative pose with the lowest cumulative distance to all other frames in cluster was extracted. A cluster may comprise snapshots from 1 or more trajectories of final 10 ns. When a cluster is represented by more than one trajectory, only the 10 ns from the trajectory with the lowest enthalpy was used to rank this cluster/pose. The top 5 poses extracted from the top 5 clusters based on MMGBSA energy of the trajectory was used for rescoring by HAPOD. Using the best consecutive 10 ns is the unified selection criteria we have established for prescoring, which also streamlines the process to perform with many trajectories. Clusters that are only from a portion of a trajectory significantly smaller than 10 ns indicate pose instability. Their corresponding trajectories generally had poor MMGBSA energies and they were therefore eliminated in this stage. Even occasionally when a trajectory with a poorly formed cluster was within the top 5 in energy (i.e., **Figure 3**, 5T35 1.1 and **Figure S9**, 6HAX 1.20), we maintained the same prescoring criteria.

MMGBSA Prescore

We use the well-established and commonly applied MMGBSA energy calculation method for initial scoring of PROTAC ternary poses here.[38, 66, 67] Typically for evaluating relative favorability of ligand-receptor binary systems, we expand the MMGBSA application to the PROTAC ternary system here.

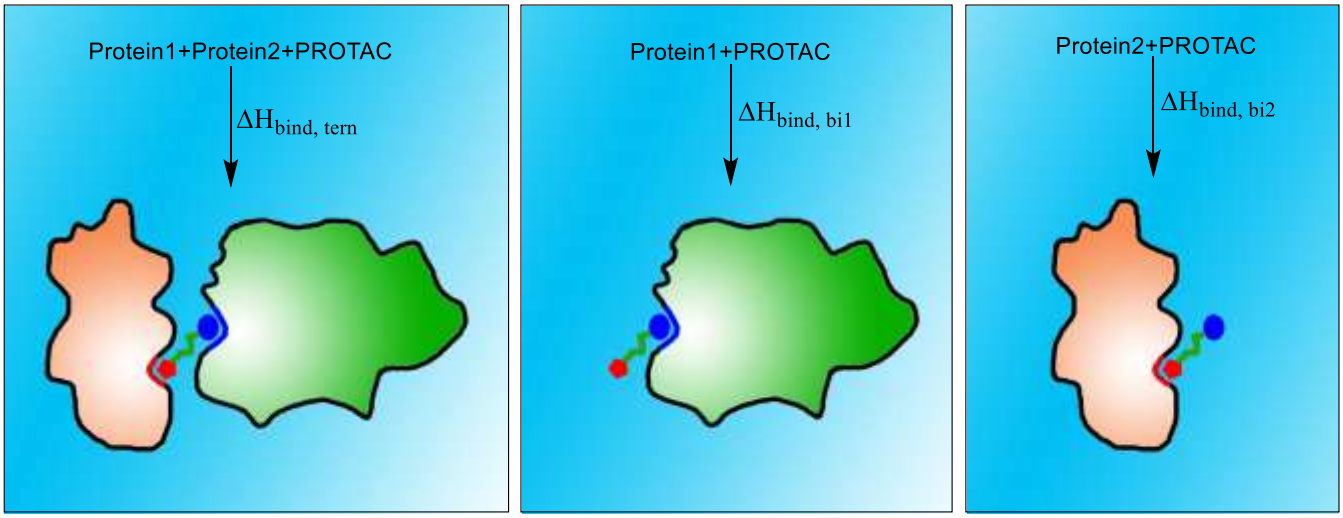

Scheme 2. Aqueous binding energy scheme for calculating ternary binding energy $\Delta H_{bind,tern}$ and cooperativity binding energy $\Delta\Delta H$ in equations (2)-(4).

$$\Delta H_{bind,tern} = H_{complex} - H_{protein1} - H_{PROTAC} - H_{protein2} \quad (2)$$

$$\Delta H_{bind,coop}(\Delta\Delta H) = \Delta H_{bind,tern} - \Delta H_{bind,bi1} - \Delta H_{bind,bi2} \quad (3)$$

$$= (H_{complex} - H_{protein1} - H_{PROTAC} - H_{protein2}) - (H_{bi1} - H_{protein1} - H_{PROTAC}) - (H_{bi2} - H_{protein2} - H_{PROTAC})$$

$$= H_{complex} + H_{PROTAC} - H_{bi1} - H_{bi2} \quad (4)$$

Using the GB^{OBC2} (igb=5) model with mbondi2 radii,[68] the last 10 ns of each trajectory was subject to MMGBSA scoring of ternary binding energies, as in eq. (2). With MMPBSA.py,[69] for each single trajectory the program was run 3 times, each time having the PROTAC, protein1 or protein2 defined as

the ligand, and the remaining two components as the receptor. The required parameter-topology files for each run were stripped from that of the complex by *cpptraj*.

In addition to ternary binding energy, cooperativity binding energy is a common parameter for PROTAC ternary binding systems.[46, 70] The ternary binding energy may be very favorable if protein affinity with a single ligand warhead happens to be very strong, but it does not completely reflect the stability of the ternary system. Therefore, we want to separately subtract all PROTAC-single protein binding energies from the total ternary binding energy as a second measure, ΔΔH, as in eq. (3) or simplified as eq. (4). This is the same energy as defined and measured by Roy and Ciulli et al. by SPR.[70] When comparing poses for ranking, both ΔH and ΔΔH were considered by simply summing up of the two to get a combined H score.

Final Rescore by Heating-Accelerated Pose Departure Trials (HAPOD)

HAPOD Simulations. To perform our heating-accelerated pose departure (HAPOD) analysis for PROTAC ternary poses we generated, the clustering and MMGBSA provided a preliminary ranking of the candidate ternary poses (**Table 2**). For each system, a minimum of top 5 poses based on their corresponding H score are taken for the final rescoring. These extracted candidate poses were used as the starting frame in the heating. Only the two proteins and PROTAC were retained in the pose. Any pose from any method of sampling can be fed into this step, such as crystal poses (**Figure 5**) or PRosetttaC poses (**Figure 6**).

Before heating, all poses were reassigned AM1-BCC partial charges for the PROTAC and prepared with the same *tleap* workflow as for the MD relaxations. HMR was applied. The same minimization and equilibration procedure was used as in the "Explicit solvent MD trials" section. The production stage of 25 ns was run in the NPT ensemble (Langevin thermostat, ntt=3, gamma_ln=0.01, Monte Carlo barostat,

ntb=2, ntp=1, barostat=2, taup=0.5). The long-distance cutoff was set to 8 Å. The SHAKE algorithm was used. The timestep was set to 0.002 ps, and snapshots recorded every 0.05 ns.

Generating scores from HAPOD. With the smaller protein (BRD4 or BD) and its ligand warhead aligned to the starting pose, the RMSD of the other side to its start was measured as an indicator of movement and stability. One could either measure the core regions of the other protein or the other ligand warhead, given their correlated positions. We measured the other ligand warhead. One example is shown in **Figure 8**.

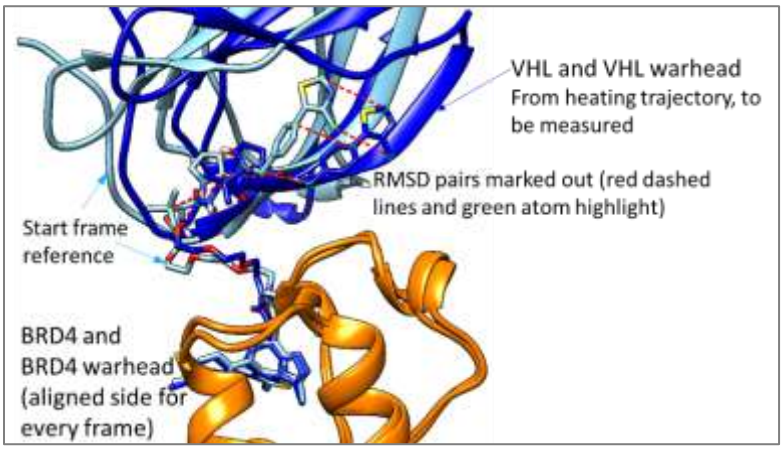

Figure 8. One example taken from 5T35 heating rescore trails. Representative heavy atoms on the unaligned ligand warhead (dark blue) were measured to the candidate pose (start) in terms of per-frame RMSD.

To convert the RMSDs into a final score indicating ternary pose stability, we evaluated it in two ways, and generated an occupancy score and temperature (T) score. The occupancy score represents the time fraction of the moving PROTAC end being within 3.5 Å of the starting pose over the course of 25 ns. With 500 frames in total for 25 ns, the total number of frames that had a 10-frame moving average of < 3.5 Å RMSD to the start are counted and divided by 20. This is the occupancy time duration in ns, and this value is divided by 25 and multiplied by 100 to give a range of 0-100. For the T score, when this same moving average RMSD increased to ≥ 4 Å, the thermostat temperature is recorded. If the RMSD falls

back to moving average < 3 Å later in the trajectory, the thermostat temperature is recorded again when the next time it crosses to ≥ 4 Å. If by the end of the heating scheme, the RMSD has never crossed over 4 Å, or fell back to less than 3 Å and have not crossed over 4 Å yet, then a 420 thermostat temperature is recorded for this instance. For each trajectory, all recorded thermostat temperatures are averaged to give a single T score. The 10 T scores from the 10 replicates are then averaged again, as well as the 10 occupancy scores. For two reasons, the heating is not performed at temperatures higher than 410 K. 1) The non-native poses rarely reached 410 K and still remained undeparted. Only some crystal poses could be heated to 410 K without the pose departure occurring. The difference is already obvious. 2) The increased likelihood of protein unfolding at high temperature may tend to make all poses look like negative ones. When performing the RMSD measurements, in addition to the indicated region in **Figure 8**, the unaligned protein, linker, aligned ligand warhead and aligned protein were all plotted as control measures to monitor potential abnormalities and other signs of instability, such as protein unfolding and ligand dissociation from pocket. Fortunately, these events were rarely seen, which indicated that the situation was not complicated by these factors.

HAPOD scoring on poses generated from other sources. Ternary docking poses from other sources can also be fed into the heating step for final rescoring. To demonstrate independent usage, systems and poses generated and reported by the PRosettaC study[10, 37] were taken for rescoring with our HAPOD method. In the reported study, ternary poses were clustered, and their scoring criteria was cluster population rank. Of the 10 PDB systems studied with the reported method in literature, two systems had the near-native pose as the top cluster, and four systems had it ranked 2 or 3 (**Figure 1b**). MMGBSA binding energy followed by HAPOD scores were evaluated for their poses generated for 6BOY and 6HAY, each representing a good but not perfect, and poorer but not worst system. For the non-native poses, a single pose was chosen from each cluster. For the native pose control, 6BOY poses from the found near-native cluster (no.2) were

compared to the crystal native pose and the one closest to the crystal was used. In 6HAY the near-native cluster (no.20) was only a singleton and was used directly. The native crystal itself as the starting point was also used in both systems.

For calculating singe-frame MMGBSA binding energies, each pose was subject to the same MD preparation steps as described previously for the explicit solvent runs. To minimize the structure, heavy atoms restrained at 5 kcal/mol/Å, 5,000 steps of steepest descent minimization was performed, followed by another 5,000 steps with the restraint weight relaxed to 1 kcal/mol/Å, followed by another 5,000 steps with no restraints. Afterwards, conjugate gradient minimization was applied for a final 5,000 steps. From this single minimized frame, the MMGBSA energies were calculated the same way as described previously in the MMGBSA prescore section.

For poses taken for the HAPOD rescore after the initial MMGBSA energy calculations, the occupancy score and T score were obtained in the same way as previously described.

Wall Time of HAPOD

For each of the 25 ns heating runs under the conditions reported here, on an NVIDIA GeForce RTX 2080Ti GPU, the smaller VHL systems take about 3-4 hours, and the larger CRBN systems take about 6-7 hours. This is well suited for parallel running.

ASSOCIATED CONTENT

Supporting Information.

Step-by-step model building procedures with UCSF Chimera.

Additional data and results.

Provided in GitHub repository.

Input structures and scripts used throughout the whole study, as well as output files and results. https://github.com/JL2021MD/PROTACModeling.git

AUTHOR INFORMATION

***Corresponding Authors**

Spencer S. Ericksen

E-mail: sseric ksen@wisc.edu

Weiping Tang

E-mail: weiping.tang@wisc.edu

Notes

The authors declare no competing financial interest.

ACKNOWLEDGMENT

We would like to thank Dr. Xuhui Huang from the University of Wisconsin-Madison for valuable discussions and inputs. Support for this research was provided by the University of Wisconsin - Madison Office of the Vice Chancellor for Research and Graduate Education with funding from the Wisconsin Alumni Research Foundation through a UW2020 award.

With the exception of the pretest results generated on a workstation with a single GPU, the majority of the compute-intensive work was performed using the computing resources and assistance of the UW-Madison Center for High Throughput Computing (CHTC) in the Department of Computer Sciences. The CHTC is supported by UW-Madison, the Advanced Computing Initiative, the Wisconsin Alumni Research Foundation, the Wisconsin Institutes for Discovery, and the National Science Foundation, and is an active member of the Open Science Grid, which is supported by the National Science Foundation and the U.S. Department of Energy's Office of Science. Molecular graphics images were produced using the UCSF Chimera package from the Resource for Biocomputing, Visualization, and Informatics at the University of California, San Francisco with support from NIH P41-GM103311.

REFERENCES

1. Bondeson, D. P.; Mares, A.; Smith, I. E. D.; Ko, E.; Campos, S.; Miah, A. H.; Mulholland, K. E.; Routly, N.; Buckley, D. L.; Gustafson, J. L.; Zinn, N.; Grandi, P.; Shimamura, S.; Bergamini, G.; Faelth-Savitski, M.; Bantscheff, M.; Cox, C.; Gordon, D. A.; Willard, R. R.; Flanagan, J. J.; Casillas, L. N.; Votta, B. J.; den Besten, W.; Famm, K.; Kruidenier, L.; Carter, P. S.; Harling, J. D.; Churcher, I.; Crews, C. M., Catalytic in vivo protein knockdown by small-molecule PROTACs. *Nat. Chem. Biol.* **2015,** *11* (8), 611-617.
2. Winter, G. E.; Buckley, D. L.; Paulk, J.; Roberts, J. M.; Souza, A.; Dhe-Paganon, S.; Bradner, J. E., Phthalimide conjugation as a strategy for in vivo target protein degradation. *Science* **2015,** *348* (6241), 1376.
3. Burslem, G. M.; Crews, C. M., Proteolysis-Targeting Chimeras as Therapeutics and Tools for Biological Discovery. *Cell* **2020,** *181* (1), 102-114.
4. Salami, J.; Crews, C. M., Waste disposal—An attractive strategy for cancer therapy. *Science* **2017,** *355* (6330), 1163.
5. Lai, A. C.; Crews, C. M., Induced protein degradation: an emerging drug discovery paradigm. *Nat. Rev. Drug Discovery* **2017,** *16* (2), 101-114.
6. Wan, Y.; Yan, C.; Gao, H.; Liu, T., Small-molecule PROTACs: novel agents for cancer therapy. *Future Med. Chem.* **2020,** *12* (10), 915-938.
7. Konstantinidou, M.; Li, J.; Zhang, B.; Wang, Z.; Shaabani, S.; Ter Brake, F.; Essa, K.; Dömling, A., PROTACs– a game-changing technology. *Expert Opin. Drug Discov.* **2019,** *14* (12), 1255-1268.
8. Drummond, M. L.; Williams, C. I., In Silico Modeling of PROTAC-Mediated Ternary Complexes: Validation and Application. *J. Chem. Inf. Model.* **2019,** *59* (4), 1634-1644.
9. Drummond, M. L.; Henry, A.; Li, H.; Williams, C. I., Improved Accuracy for Modeling PROTAC-Mediated Ternary Complex Formation and Targeted Protein Degradation via New In Silico Methodologies. *J. Chem. Inf. Model.* **2020,** *60* (10), 5234-5254.
10. Zaidman, D.; Prilusky, J.; London, N., PRosettaC: Rosetta Based Modeling of PROTAC Mediated Ternary Complexes. *J. Chem. Inf. Model.* **2020**.
11. Araki, M.; Matsumoto, S.; Bekker, G.-J.; Isaka, Y.; Sagae, Y.; Kamiya, N.; Okuno, Y., Exploring ligand binding pathways on proteins using hypersound-accelerated molecular dynamics. *Nat. Commun.* **2021,** *12* (1), 2793.
12. Salmaso, V.; Moro, S., Bridging Molecular Docking to Molecular Dynamics in Exploring Ligand-Protein Recognition Process: An Overview. *Front. Pharmacol.* **2018,** *9* (923).
13. Kappel, K.; Miao, Y.; McCammon, J. A., Accelerated molecular dynamics simulations of ligand binding to a muscarinic G-protein-coupled receptor. *Q. Rev. Biophys.* **2015,** *48* (4), 479-487.
14. Asciutto, E. K.; Kopanchuk, S.; Lepland, A.; Simón-Gracia, L.; Aleman, C.; Teesalu, T.; Scodeller, P., Phage-Display-Derived Peptide Binds to Human CD206 and Modeling Reveals a New Binding Site on the Receptor. *J. Phys. Chem.* **2019,** *123* (9), 1973-1982.
15. Coveney, P. V.; Wan, S., On the calculation of equilibrium thermodynamic properties from molecular dynamics. *Phys. Chem. Chem. Phys.* **2016,** *18* (44), 30236-30240.
16. Mayor, U.; Johnson, C. M.; Daggett, V.; Fersht, A. R., Protein folding and unfolding in microseconds to nanoseconds by experiment and simulation. *Proc. Natl. Acad. Sci.* **2000,** *97* (25), 13518.
17. Mayor, U.; Guydosh, N. R.; Johnson, C. M.; Grossmann, J. G.; Sato, S.; Jas, G. S.; Freund, S. M. V.; Alonso, D. O. V.; Daggett, V.; Fersht, A. R., The complete folding pathway of a protein from nanoseconds to microseconds. *Nature* **2003,** *421* (6925), 863-867.
18. Rocco, A. G.; Mollica, L.; Ricchiuto, P.; Baptista, A. M.; Gianazza, E.; Eberini, I., Characterization of the Protein Unfolding Processes Induced by Urea and Temperature. *Biophys. J.* **2008,** *94* (6), 2241-2251.
19. Settanni, G.; Fersht, A. R., High Temperature Unfolding Simulations of the TRPZ1 Peptide. *Biophys. J.* **2008,** *94* (11), 4444-4453.

20. Pierce, L. C. T.; Salomon-Ferrer, R.; Augusto F de Oliveira, C.; McCammon, J. A.; Walker, R. C., Routine Access to Millisecond Time Scale Events with Accelerated Molecular Dynamics. *J. Chem. Theory Comput.* **2012,** *8* (9), 2997-3002.
21. Tiwary, P.; Limongelli, V.; Salvalaglio, M.; Parrinello, M., Kinetics of protein–ligand unbinding: Predicting pathways, rates, and rate-limiting steps. *Proc. Natl. Acad. Sci.* **2015,** *112* (5), E386.
22. Mollica, L.; Decherchi, S.; Zia, S. R.; Gaspari, R.; Cavalli, A.; Rocchia, W., Kinetics of protein-ligand unbinding via smoothed potential molecular dynamics simulations. *Sci. Rep.* **2015,** *5* (1), 11539.
23. Miao, Y.; Feher, V. A.; McCammon, J. A., Gaussian Accelerated Molecular Dynamics: Unconstrained Enhanced Sampling and Free Energy Calculation. *J. Chem. Theory Comput.* **2015,** *11* (8), 3584-3595.
24. Deb, I.; Frank, A. T., Accelerating Rare Dissociative Processes in Biomolecules Using Selectively Scaled MD Simulations. *J. Chem. Theory Comput.* **2019,** *15* (11), 5817-5828.
25. Wolf, S.; Lickert, B.; Bray, S.; Stock, G., Multisecond ligand dissociation dynamics from atomistic simulations. *Nat. Commun.* **2020,** *11* (1), 2918.
26. Gadd, M. S.; Testa, A.; Lucas, X.; Chan, K.-H.; Chen, W.; Lamont, D. J.; Zengerle, M.; Ciulli, A., Structural basis of PROTAC cooperative recognition for selective protein degradation. *Nat. Chem. Biol.* **2017,** *13* (5), 514-521.
27. Weng, G.; Li, D.; Kang, Y.; Hou, T., Integrative Modeling of PROTAC-Mediated Ternary Complexes. *J. Med. Chem.* **2021,** *64* (21), 16271-16281.
28. Izadi, S.; Anandakrishnan, R.; Onufriev, A. V., Implicit Solvent Model for Million-Atom Atomistic Simulations: Insights into the Organization of 30-nm Chromatin Fiber. *J. Chem. Theory Comput.* **2016,** *12* (12), 5946-5959.
29. Nguyen, H.; Maier, J.; Huang, H.; Perrone, V.; Simmerling, C., Folding Simulations for Proteins with Diverse Topologies Are Accessible in Days with a Physics-Based Force Field and Implicit Solvent. *J. Am. Chem. Soc.* **2014,** *136* (40), 13959-13962.
30. Sun, Z.; Yan, Y. N.; Yang, M.; Zhang, J. Z. H., Interaction entropy for protein-protein binding. *J. Chem. Phys.* **2017,** *146* (12), 124124.
31. Genheden, S.; Kuhn, O.; Mikulskis, P.; Hoffmann, D.; Ryde, U., The Normal-Mode Entropy in the MM/GBSA Method: Effect of System Truncation, Buffer Region, and Dielectric Constant. *J. Chem. Inf. Model.* **2012,** *52* (8), 2079-2088.
32. Lawrenz, M.; Baron, R.; McCammon, J. A., Independent-Trajectories Thermodynamic-Integration Free-Energy Changes for Biomolecular Systems: Determinants of H5N1 Avian Influenza Virus Neuraminidase Inhibition by Peramivir. *J. Chem. Theory Comput.* **2009,** *5* (4), 1106-1116.
33. Steinbrecher, T.; Case, D. A.; Labahn, A., Free energy calculations on the binding of novel thiolactomycin derivatives to E. coli fatty acid synthase I. *Bioorg. Med. Chem.* **2012,** *20* (11), 3446-3453.
34. Genheden, S.; Ryde, U., The MM/PBSA and MM/GBSA methods to estimate ligand-binding affinities. *Expert Opin. Drug Discov.* **2015,** *10* (5), 449-461.
35. Dragovich, P. S.; Pillow, T. H.; Blake, R. A.; Sadowsky, J. D.; Adaligil, E.; Adhikari, P.; Chen, J.; Corr, N.; dela Cruz-Chuh, J.; Del Rosario, G.; Fullerton, A.; Hartman, S. J.; Jiang, F.; Kaufman, S.; Kleinheinz, T.; Kozak, K. R.; Liu, L.; Lu, Y.; Mulvihill, M. M.; Murray, J. M.; O'Donohue, A.; Rowntree, R. K.; Sawyer, W. S.; Staben, L. R.; Wai, J.; Wang, J.; Wei, B.; Wei, W.; Xu, Z.; Yao, H.; Yu, S.-F.; Zhang, D.; Zhang, H.; Zhang, S.; Zhao, Y.; Zhou, H.; Zhu, X., Antibody-Mediated Delivery of Chimeric BRD4 Degraders. Part 2: Improvement of In Vitro Antiproliferation Activity and In Vivo Antitumor Efficacy. *J. Med. Chem.* **2021,** *64* (5), 2576-2607.
36. https://github.com/JL2021MD/PROTACModeling.git.
37. Nir, Z. D. L., Results files of PRosettac for the following PDBs: 5T35, 6BOY, 6BN7, 6BN8, 6BN9, 6BNB, 6HAX, 6HAY, 6HR2, 6SIS. https://zenodo.org/record/3967246/files/Bound_Clusters.zip.
38. Wang, E.; Sun, H.; Wang, J.; Wang, Z.; Liu, H.; Zhang, J. Z. H.; Hou, T., End-Point Binding Free Energy Calculation with MM/PBSA and MM/GBSA: Strategies and Applications in Drug Design. *Chem. Rev.* **2019,** *119* (16), 9478-9508.

39. Kuhn, B.; Gerber, P.; Schulz-Gasch, T.; Stahl, M., Validation and Use of the MM-PBSA Approach for Drug Discovery. *J. Med. Chem.* **2005,** *48* (12), 4040-4048.
40. Sun, H.; Li, Y.; Tian, S.; Xu, L.; Hou, T., Assessing the performance of MM/PBSA and MM/GBSA methods. 4. Accuracies of MM/PBSA and MM/GBSA methodologies evaluated by various simulation protocols using PDBbind data set. *Phys. Chem. Chem. Phys.* **2014,** *16* (31), 16719-16729.
41. Jumper, J.; Evans, R.; Pritzel, A.; Green, T.; Figurnov, M.; Ronneberger, O.; Tunyasuvunakool, K.; Bates, R.; Žídek, A.; Potapenko, A.; Bridgland, A.; Meyer, C.; Kohl, S. A. A.; Ballard, A. J.; Cowie, A.; Romera-Paredes, B.; Nikolov, S.; Jain, R.; Adler, J.; Back, T.; Petersen, S.; Reiman, D.; Clancy, E.; Zielinski, M.; Steinegger, M.; Pacholska, M.; Berghammer, T.; Bodenstein, S.; Silver, D.; Vinyals, O.; Senior, A. W.; Kavukcuoglu, K.; Kohli, P.; Hassabis, D., Highly accurate protein structure prediction with AlphaFold. *Nature* **2021,** *596* (7873), 583-589.
42. Kozakov, D.; Hall, D. R.; Xia, B.; Porter, K. A.; Padhorny, D.; Yueh, C.; Beglov, D.; Vajda, S., The ClusPro web server for protein–protein docking. *Nat. Protoc.* **2017,** *12* (2), 255-278.
43. Vajda, S.; Yueh, C.; Beglov, D.; Bohnuud, T.; Mottarella, S. E.; Xia, B.; Hall, D. R.; Kozakov, D., New additions to the ClusPro server motivated by CAPRI. *Proteins: Struct., Funct., Bioinf.* **2017,** *85* (3), 435-444.
44. Kozakov, D.; Beglov, D.; Bohnuud, T.; Mottarella, S. E.; Xia, B.; Hall, D. R.; Vajda, S., How good is automated protein docking? *Proteins: Struct., Funct., Bioinf.* **2013,** *81* (12), 2159-2166.
45. Testa, A.; Hughes, S. J.; Lucas, X.; Wright, J. E.; Ciulli, A., Structure-Based Design of a Macrocyclic PROTAC. *Angew. Chem. Int. Ed.* **2020,** *59* (4), 1727-1734.
46. Nowak, R. P.; DeAngelo, S. L.; Buckley, D.; He, Z.; Donovan, K. A.; An, J.; Safaee, N.; Jedrychowski, M. P.; Ponthier, C. M.; Ishoey, M.; Zhang, T.; Mancias, J. D.; Gray, N. S.; Bradner, J. E.; Fischer, E. S., Plasticity in binding confers selectivity in ligand-induced protein degradation. *Nat. Chem. Biol.* **2018,** *14* (7), 706-714.
47. Farnaby, W.; Koegl, M.; Roy, M. J.; Whitworth, C.; Diers, E.; Trainor, N.; Zollman, D.; Steurer, S.; Karolyi-Oezguer, J.; Riedmueller, C.; Gmaschitz, T.; Wachter, J.; Dank, C.; Galant, M.; Sharps, B.; Rumpel, K.; Traxler, E.; Gerstberger, T.; Schnitzer, R.; Petermann, O.; Greb, P.; Weinstabl, H.; Bader, G.; Zoephel, A.; Weiss-Puxbaum, A.; Ehrenhöfer-Wölfer, K.; Wöhrle, S.; Boehmelt, G.; Rinnenthal, J.; Arnhof, H.; Wiechens, N.; Wu, M.-Y.; Owen-Hughes, T.; Ettmayer, P.; Pearson, M.; McConnell, D. B.; Ciulli, A., BAF complex vulnerabilities in cancer demonstrated via structure-based PROTAC design. *Nat. Chem. Biol.* **2019,** *15* (7), 672-680.
48. Hawkins, P. C. D.; Skillman, A. G.; Warren, G. L.; Ellingson, B. A.; Stahl, M. T., Conformer Generation with OMEGA: Algorithm and Validation Using High Quality Structures from the Protein Databank and Cambridge Structural Database. *J. Chem. Inf. Model.* **2010,** *50* (4), 572-584.
49. *OMEGA 4.1.1.1: OpenEye Scientific Software*, Santa Fe, NM. http://www.eyesopen.com.
50. Pettersen, E. F.; Goddard, T. D.; Huang, C. C.; Couch, G. S.; Greenblatt, D. M.; Meng, E. C.; Ferrin, T. E., UCSF Chimera--a visualization system for exploratory research and analysis. *J. Comput. Chem.* **2004,** *25* (13), 1605-12.
51. Wang, J.; Wang, W.; Kollman, P. A.; Case, D. A., Automatic atom type and bond type perception in molecular mechanical calculations. *J. Mol. Graphics Model.* **2006,** *25* (2), 247-260.
52. Tian, C.; Kasavajhala, K.; Belfon, K. A. A.; Raguette, L.; Huang, H.; Migues, A. N.; Bickel, J.; Wang, Y.; Pincay, J.; Wu, Q.; Simmerling, C., ff19SB: Amino-Acid-Specific Protein Backbone Parameters Trained against Quantum Mechanics Energy Surfaces in Solution. *J. Chem. Theory Comput.* **2020,** *16* (1), 528-552.
53. Izadi, S.; Anandakrishnan, R.; Onufriev, A. V., Building Water Models: A Different Approach. *The Journal of Physical Chemistry Letters* **2014,** *5* (21), 3863-3871.
54. Joung, I. S.; Cheatham, T. E., Determination of Alkali and Halide Monovalent Ion Parameters for Use in Explicitly Solvated Biomolecular Simulations. *J. Phys. Chem.* **2008,** *112* (30), 9020-9041.
55. Hopkins, C. W.; Le Grand, S.; Walker, R. C.; Roitberg, A. E., Long-Time-Step Molecular Dynamics through Hydrogen Mass Repartitioning. *J. Chem. Theory Comput.* **2015,** *11* (4), 1864-1874.

56. Maier, J. A.; Martinez, C.; Kasavajhala, K.; Wickstrom, L.; Hauser, K. E.; Simmerling, C., ff14SB: Improving the Accuracy of Protein Side Chain and Backbone Parameters from ff99SB. *J. Chem. Theory Comput.* **2015,** *11* (8), 3696-3713.
57. Jorgensen, W. L.; Chandrasekhar, J.; Madura, J. D.; Impey, R. W.; Klein, M. L., Comparison of simple potential functions for simulating liquid water. *J. Chem. Phys.* **1983,** *79* (2), 926-935.
58. Onufriev, A.; Bashford, D.; Case, D. A., Exploring protein native states and large-scale conformational changes with a modified generalized born model. *Proteins: Struct., Funct., Bioinf.* **2004,** *55* (2), 383-394.
59. Knapp, B.; Ospina, L.; Deane, C. M., Avoiding False Positive Conclusions in Molecular Simulation: The Importance of Replicas. *J. Chem. Theory Comput.* **2018,** *14* (12), 6127-6138.
60. Le Grand, S.; Götz, A. W.; Walker, R. C., SPFP: Speed without compromise—A mixed precision model for GPU accelerated molecular dynamics simulations. *Comput. Phys. Commun.* **2013,** *184* (2), 374-380.
61. Salomon-Ferrer, R.; Götz, A. W.; Poole, D.; Le Grand, S.; Walker, R. C., Routine Microsecond Molecular Dynamics Simulations with AMBER on GPUs. 2. Explicit Solvent Particle Mesh Ewald. *J. Chem. Theory Comput.* **2013,** *9* (9), 3878-3888.
62. Götz, A. W.; Williamson, M. J.; Xu, D.; Poole, D.; Le Grand, S.; Walker, R. C., Routine Microsecond Molecular Dynamics Simulations with AMBER on GPUs. 1. Generalized Born. *J. Chem. Theory Comput.* **2012,** *8* (5), 1542-1555.
63. D.A. Case, K. B., I.Y. Ben-Shalom, S.R. Brozell, D.S. Cerutti, T.E. Cheatham, III, V.W.D. Cruzeiro,; T.A. Darden, R. E. D., G. Giambasu, M.K. Gilson, H. Gohlke, A.W. Goetz,R Harris, S. Izadi, S.A. Iz-; mailov, K. K., A. Kovalenko, R. Krasny, T. Kurtzman, T.S. Lee, S. LeGrand, P. Li, C. Lin, J. Liu,; T. Luchko, R. L., V. Man, K.M. Merz, Y. Miao, O. Mikhailovskii, G. Monard, H. Nguyen, A. Onufriev, F.; Pan, S. P., R. Qi, D.R. Roe, A. Roitberg, C. Sagui, S. Schott-Verdugo, J. Shen, C.L. Simmerling, N.R.; Skrynnikov, J. S., J. Swails, R.C. Walker, J. Wang, L. Wilson, R.M. Wolf, X. Wu, Y. Xiong, Y. Xue,; Kollman, D. M. Y. a. P. A. *AMBER 2020*, University of California, San Francisco., 2020.
64. Carrascal, N.; Rizzo, R. C., Calculation of binding free energies for non-zinc chelating pyrimidine dicarboxamide inhibitors with MMP-13. *Bioorg. Med. Chem. Lett.* **2009,** *19* (1), 47-50.
65. Roe, D. R.; Cheatham, T. E., PTRAJ and CPPTRAJ: Software for Processing and Analysis of Molecular Dynamics Trajectory Data. *J. Chem. Theory Comput.* **2013,** *9* (7), 3084-3095.
66. Still, W. C.; Tempczyk, A.; Hawley, R. C.; Hendrickson, T., Semianalytical treatment of solvation for molecular mechanics and dynamics. *J. Am. Chem. Soc.* **1990,** *112* (16), 6127-6129.
67. Hou, T.; Wang, J.; Li, Y.; Wang, W., Assessing the Performance of the MM/PBSA and MM/GBSA Methods. 1. The Accuracy of Binding Free Energy Calculations Based on Molecular Dynamics Simulations. *J. Chem. Inf. Model.* **2011,** *51* (1), 69-82.
68. Onufriev, A.; Case, D. A.; Bashford, D., Effective Born radii in the generalized Born approximation: the importance of being perfect. *J. Comput. Chem.* **2002,** *23* (14), 1297-304.
69. Miller, B. R.; McGee, T. D.; Swails, J. M.; Homeyer, N.; Gohlke, H.; Roitberg, A. E., MMPBSA.py: An Efficient Program for End-State Free Energy Calculations. *J. Chem. Theory Comput.* **2012,** *8* (9), 3314-3321.
70. Roy, M. J.; Winkler, S.; Hughes, S. J.; Whitworth, C.; Galant, M.; Farnaby, W.; Rumpel, K.; Ciulli, A., SPR-Measured Dissociation Kinetics of PROTAC Ternary Complexes Influence Target Degradation Rate. *ACS Chem. Biol.* **2019,** *14* (3), 361-368.

Table of Contents graphic: